Check for updates

View Article Online
View Journal

Soft Matter

Accepted Manuscript

This article can be cited before page numbers have been issued, to do this please use: A. Gas, L. Keiser, C. Clanet and D. Quéré, *Soft Matter*, 2017, DOI: 10.1039/C7SM01226H.

This is an Accepted Manuscript, which has been through the Royal Society of Chemistry peer review process and has been accepted for publication.

Accepted Manuscripts are published online shortly after acceptance, before technical editing, formatting and proof reading. Using this free service, authors can make their results available to the community, in citable form, before we publish the edited article. We will replace this Accepted Manuscript with the edited and formatted Advance Article as soon as it is available.

You can find more information about Accepted Manuscripts in the author guidelines.

Please note that technical editing may introduce minor changes to the text and/or graphics, which may alter content. The journal's standard Terms & Conditions and the ethical guidelines, outlined in our author and reviewer resource centre, still apply. In no event shall the Royal Society of Chemistry be held responsible for any errors or omissions in this Accepted Manuscript or any consequences arising from the use of any information it contains.

ROYAL SOCIETY OF CHEMISTRY

rsc.li/soft-matter-journal

View Article Online
DOI: 10.1039/C7SM01226H

Published on 08 September 2017. Downloaded by University of Cambridge on 15/09/2017 15:34:56.

Drop friction on liquid-infused materials

Armelle Keiser[1,2], Ludovic Keiser[1,3], Christophe Clanet[1,2] & David Quéré[1,2]

1. Physique et Mécanique des Milieux Hétérogènes, UMR 7636 du CNRS, ESPCI, 75005 Paris, France.
2. LadHyX, UMR 7646 du CNRS, École polytechnique, 91128 Palaiseau, France.
3. Total S.A., Pôle d'Études et de Recherche de Lacq, BP 47, 64170 Lacq, France.

We discuss in this paper the nature of the friction generated as a drop glides on a textured material infused by another liquid. Different regimes are found, depending on the viscosities of both liquids. While a viscous drop simply obeys a Stokes-type friction, the force opposing a drop moving on a viscous substrate becomes non-linear in velocity. A liquid on an infused material is surrounded by a meniscus, and this specific feature is proposed to be responsible for the special frictions observed on both adhesive and non-adhesive substrates.

Soft Matter Accepted Manuscript

View Article Online
DOI: 10.1039/C7SM01226H

Published on 08 September 2017. Downloaded by University of Cambridge on 15/09/2017 15:34:56.

Liquid droplets on solids generally have high adhesion and friction, owing to the contact line bounding them. This line can pin on defects [1], and its presence enhances dissipation as the liquid moves [2-3]. In order to promote mobility, it was proposed to lubricate the gap between the solid substrate and the moving drop. The lubrication layer may consist either of air (Leidenfrost state [4], superhydrophobic solids [5-6]), or of another liquid (here called oil) trapped by textures [7] or magnetically [8] – all kinds of situations of practical interest, since they provide anti-biofouling [9], anti-dew [10-11], or even anti-ice abilities [12-14]. This idea has been widely exploited by nature, with multiple examples of peculiar plants [15] having water-repellent leaves [16] or slippery surfaces [17-18]. By combining textures and chemistry, these plants get remarkable non-adhesive properties, making them able to fully repel water (lotus leaf), or to trap insects owing to water filmification (carnivorous Nepenthes). We focus here on oil-infused textured materials, which were shown to display spectacular slippery behaviours [19-21]. These materials are made in two steps: firstly, a solid is decorated by hydrophobic micro-textures; secondly, oil is infused by spontaneous impregnation [22] or dip-coating [21, 23]. If the texture, surface chemistry and oil are carefully combined, a drop of water (possibly mixed with glycerol or hydrosoluble polymers) will stay at the surface of the oil, and benefit from its lubricating action [24-25]. Contact angle hysteresis is minimized, and so is its adhesion to the substrate, despite apparent contact angles often close to 90° [19-21, 25]. Hence such drops easily run down inclines (as long as oil remains trapped in the textures), and we discuss here the associated friction. Depending on the liquids and texture, several kinds of dissipation can be generated, which can be exploited to tune the drop velocity.

Our samples are covered by micro-pillars made of SU8-resin and obtained by photolithography on a silicon wafer, where they occupy a rectangular area of 8 cm x 5 cm. As shown in the Supplementary Information (SI), pillars all have a height $h = 20 \pm 3$ μm and lateral size and spacing spanning respectively between 18 and 185 μm, and between 15 and 60 μm. Hence the pillar density ϕ ranges between 23% and 67%. We did experiments either with simple pillars, or with pillars covered by a nanometric sub-structure, a system recently introduced by Guan *et al.* [26]. For this purpose, we coat the textured substrate with a solution of Glaco Mirror Coat (Soft 99), let the solvent (isopropanol) evaporate, and consolidate the sample by heating it at 150°C for 20 minutes, which leaves a layer of hydrophobic nanobeads (size: 30 nm) attached to the substrate and to the pillars.

Soft Matter Accepted Manuscript

View Article Online
DOI: 10.1039/C7SM01226H

The lubricant is a silicone oil with viscosity η_o ranging between 5 mPa.s and 1000 mPa.s, with a nearly constant surface tension $\gamma_o \approx 20$ mN/m and density $\rho_o \approx 980$ kg/m^3. Silicone oil completely wets silicon and resin, so that it spontaneously fills the textures: impregnation is achieved by placing the samples in contact with a bath of oil, which ensures that we do not over-impregnate the liquid-infused material. We checked that dip-coating the sample at low velocity (smaller than 20 μm/s) from a bath of oil leads to the same results, hence found to be independent of the technique used to infuse the pillars. Then, we place on the lubricated texture a drop of water/glycerol mixture (simply called water further) with a viscosity η_w ranging between 1 mPa.s (pure water) and 1000 mPa.s (pure glycerol).

The behaviour of water depends on the presence of nanobeads. On nude pillars filled with oil, water drops (volume $\Omega = 20\,\mu$L) roll off provided the sample is tilted by at least $\alpha^* = 15° \pm 3°$ for $\phi = 23\%$. As shown in the SI, α^* increases at larger ϕ. This large adhesion arises from the water/solid contacts, which induces pinning on the textures' tops [27]. On Glaco-treated pillars, the roll-off angle α^* becomes unmeasurable ($\alpha^* \approx 0$), due to the impregnation of the nanoroughness by the oil. The thin film of oil stabilized at pillars' tops isolates water from the pillars, which minimizes angle hysteresis down to non-measurable values [26].

Then, as sketched in figure 1a, we measure the drop velocity V as a function of the gravitational driving force, modulated by varying the tilt angle α (above α^*). The drop trajectory is recorded using a video-camera (Optronis, 100 to 1000 frames per second). As shown in the SI, all drops reach a constant velocity after a few centimetres of descent, as also seen in the Supplementary Movie 1. In this stationary regime, V results from a balance between gravity and friction. Side views show that drops are quasi-hemispherical (with contact radius R) and surrounded by a small oil meniscus, as sketched in figure 1a, highlighted by red circles in figure 1b, magnified in figure 1c and visible in the Supplementary Movie 2. This circular meniscus is pulled from the oil film by the vertical component of the surface tension of water [21]. Schellenberger *et al*. characterized its geometry by confocal microscopy performed on static drops [27]. The meniscus is found here to persist in dynamical conditions, which might impact the friction opposing the moving liquid.

Published on 08 September 2017. Downloaded by University of Cambridge on 15/09/2017 15:34:56.

Soft Matter Accepted Manuscript

View Article Online
DOI: 10.1039/C7SM01226H

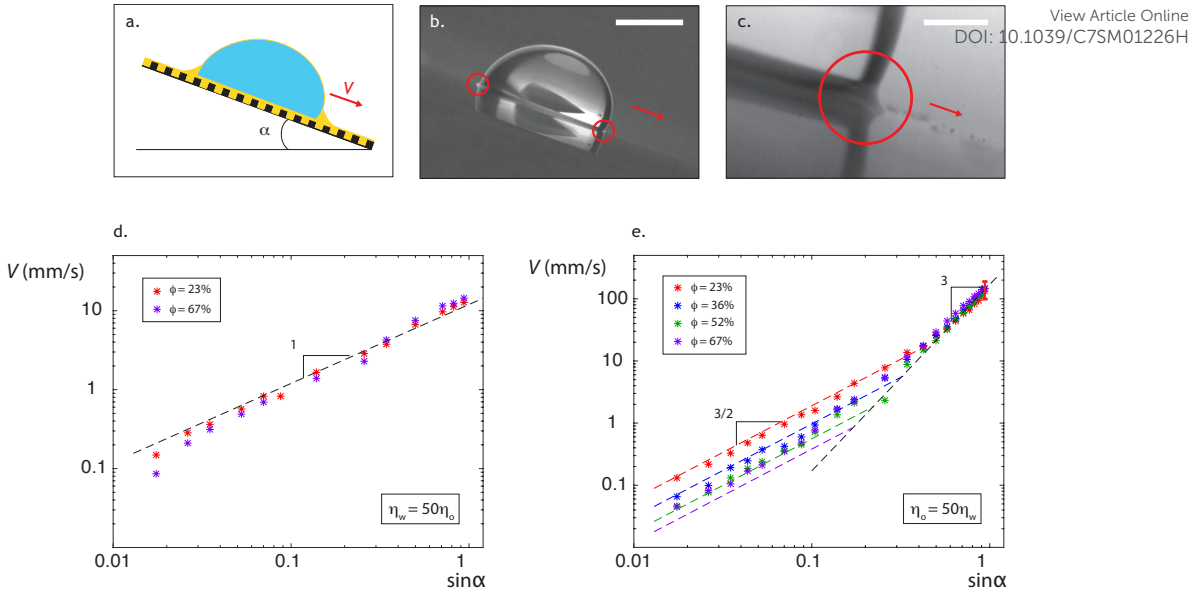

Figure 1. (a) Experimental set-up: a water drop with volume Ω runs down an oil-infused material tilted by an angle α. Its stationary speed is denoted as V. **(b)** Drop (η_w = 3 mPa.s, Ω = 20 μL) going down a silicone oil-infused surface tilted by α = 20°. The pillar density at the surface is ϕ = 23%. The scale bar shows 2 mm. **(c)** Oil front meniscus pushed by a water drop (η_w = 1 mPa.s, Ω = 20 μL) running down at V = 3 mm/s a textured material (ϕ = 23%) infused by a silicone oil (η_o = 10 mPa.s) and tilted by α = 2°. The scale bar shows 0.4 mm. **(d)** Drop speed V as a function of the driving parameter sinα, for η_o = 10 mPa.s, η_w = 500 mPa.s ($\eta_w > \eta_o$) and Ω = 20 μL. The dashed line has a slope 1. The two series of data correspond to pillar densities ϕ = 23% (red data) or ϕ = 67% (purple data). **(e)** In the opposite limit $\eta_o > \eta_w$ (here η_w = 2 mPa.s and η_o = 100 mPa.s), the drop speed becomes non-linear in driving force. Lines successively show slopes 3/2 and 3, and colors indicate the texture density (ϕ = 23%, red data; ϕ = 36%, blue data; ϕ = 52%, green data; ϕ = 67%, purple data). We indicate on the data at the largest slope the typical error bar on the velocity measurement. Colored dashed lines are positioned with the $\phi^{3/2}$- behavior predicted by eq. (3).

In order to characterize friction, we focus on the drop mobility, that is, the way speed depends on driving force. In figures 1d and 1e, the drop velocity V is plotted as a function of the sine of the tilt angle α at fixed volume Ω = 20 μL. We first consider extreme values of the ratio η_w/η_o between the liquid viscosities. (i) When water is more viscous than oil ($\eta_w = 50\eta_o$, figure 1d, supplementary movie 3), the drop speed linearly increases with the driving force, as stressed by the dashed line with slope 1 drawn across the data, and it does not depend on the texture density (the two series of data correspond to ϕ = 23% and ϕ = 67%). Hence friction is classically linear in speed (Stokes' law). (ii) When oil is more viscous than water ($\eta_o = 50\eta_w$, figure 1e, supplementary movie 1), the drop speed is not linear in driving force anymore. At small α, data can be fitted by scaling laws with power 3/2 (coloured dashed lines); in this regime, the smaller the pillar density ϕ, the quicker the motion. At large α, there is a sudden kink in the data and the velocity seems to follow a new scaling law, with an exponent 3 (black dashed line). In addition, the speed in this regime becomes independent of ϕ.

Published on 08 September 2017. Downloaded by University of Cambridge on 15/09/2017 15:34:56.

Soft Matter Accepted Manuscript

View Article Online
DOI: 10.1039/C7SM01226H

Published on 08 September 2017. Downloaded by University of Cambridge on 15/09/2017 15:34:56.

Figure 1 shows that the ratio between oil and water viscosities determines the nature of the friction. This can be directly captured by varying the drop viscosity η_w at fixed η_o. Experiments are performed for a plate inclined by $\alpha = 5°$ and a volume $\Omega = 20\ \mu$L, and results are displayed in figure 2a for $\eta_o = 10$ mPa.s (red data) and for $\eta_o = 100$ mPa.s (blue data). For each oil viscosity, two regimes are successively followed. Firstly ($\eta_w < \eta_o$), the speed V plateaus at a value roughly independent of η_w, and found to be ten times larger when η_o is ten times smaller. In this regime, dissipation then mainly occurs in oil, as already seen in figure 1e. At larger water viscosity ($\eta_w > \eta_o$, see also figure 1d), the speed becomes inversely proportional to η_w, as evidenced by the dashed lines with slope –1 (and further in figure 3).

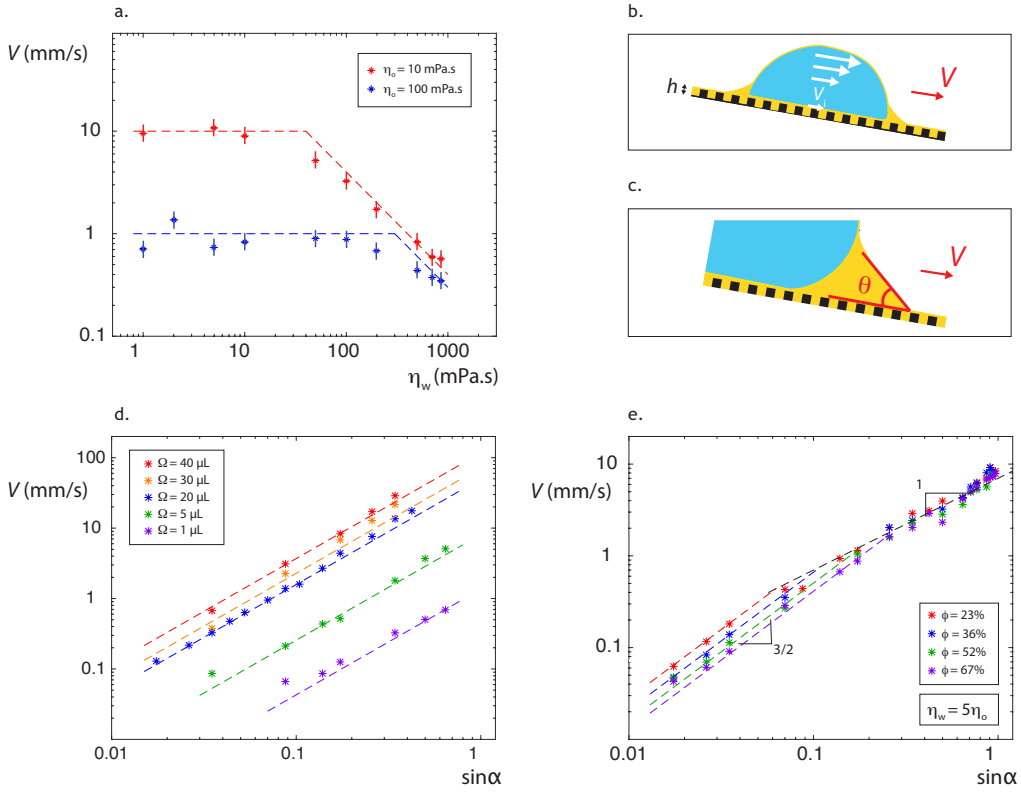

Figure 2. (a) Speed V of a descending drop ($\Omega = 20\ \mu$L) as a function of its viscosity η_w, at fixed oil viscosity ($\eta_o = 10$ mPa.s, red data; $\eta_o = 100$ mPa.s, blue data), on a substrate with $\phi = 23\%$ tilted by $\alpha = 5°$. Two regimes are successively obeyed: for $\eta_w < \eta_o$, V is independent of η_w; for $\eta_w > \eta_o$, V becomes inversely proportional to η_w (inclined lines have a slope –1). Both regimes intersect at a critical water viscosity $\eta^* \approx 3\eta_o$. **(b)** Sketch of a viscous drop going down a lubricant-impregnated surface, for which the Poiseuille flow within the drop limits the speed. We denote as V_i the velocity of the water/oil interface. **(c)** The front of the moving meniscus is dynamically deformed, with an angle $\theta(V)$. **(d)** Speed V of descending drops with viscosity $\eta_w = 2$ mPa.s and $\Omega = 1\ \mu$L (purple data), $\Omega = 5\ \mu$L (green data), $\Omega = 20\ \mu$L (blue data), $\Omega = 30\ \mu$L (orange data), $\Omega = 40\ \mu$L (red data). The surface ($\phi = 23\%$) is impregnated by oil with viscosity $\eta_o = 100$ mPa.s. **(e)** Speed V of a descending drop ($\eta_w = 500$ mPa.s) on a surface impregnated with oil of comparable viscosity ($\eta_o = 100$ mPa.s). Two regimes are successively observed, with power laws of respective exponent 3/2 and 1. Both regimes intersect at a critical speed $V^* \approx 2$ mm/s.

Soft Matter Accepted Manuscript

View Article Online
DOI: 10.1039/C7SM01226H

Friction on infused textures appears to be characterized by (at least) three different laws, a very unique situation generated by the complexity of this system. Dissipation indeed occurs in both water and oil: on the one hand, water moves inside the drop and close to the contact line; on the other hand, oil is found under the moving drop and along its edge meniscus. The existence of an underlying oil film favours slip at the oil/water interface, which we can characterize. The slip velocity V_i (defined in figure 2b) is deduced from the continuity of the viscous stress at this interface, whose scaling can be written: $\eta_w(V - V_i)/R \sim \eta_o V_i/h$, where h is the lubricant thickness. Hence we get:

$$(1) \qquad V_i \sim \frac{V}{1 + \frac{\eta_o R}{\eta_w h}}$$

The interfacial velocity V_i varies between 0 (no slip) and V (pure slip) as the slip number $\sigma = \eta_w h/\eta_o R$ increases from zero to infinity. In our case, σ is smaller than 0.1, which implies modest slip ($V_i < V/10$). Pillars should minimize even more σ: the oil film is not free, but confined within obstacles, which results in an effective oil viscosity larger than η_o [23].

We can now discuss the friction laws. As shown in experiments (figures 1d and 2a), dissipation at large η_w mainly occurs in water. In this limit, typical viscosity η_w and velocity V are respectively 500 mPa.s and a few millimetres per second, so that the corresponding Reynolds and capillary numbers are $Re = \rho RV/\eta_w \approx 10^{-3}$ and $Ca = \eta_w V/\gamma \approx 10^{-2}$, both small compared to unity. Hence dissipation has a viscous origin (figure 2a) and interfaces keep a quasi-static shape (supplementary movie 3). Owing to the presence of velocity gradients in the drop ($V_i << V$), we simply write the viscous stress in water as $\eta_w(V - V_i)/R \approx \eta_w V/R$. Once it is integrated over a surface area of order R^2, we get a force F_w scaling as $\eta_w VR$. Balancing this Stokes friction with the gravitational driving force $\rho g R^3 \sin\alpha$ yields:

$$(2) \qquad V \sim \frac{\rho g R^2}{\eta_w} \sin\alpha$$

The velocity V is proportional to the slope $\sin\alpha$ (figure 1d) and inversely proportional to the water viscosity η_w (figure 2a for $\eta_w > \eta_o$). The typical descent velocity, $V_o = \rho g R^2/\eta_w$, is

Published on 08 September 2017. Downloaded by University of Cambridge on 15/09/2017 15:34:56.

Soft Matter Accepted Manuscript

View Article Online
DOI: 10.1039/C7SM01226H

Published on 08 September 2017. Downloaded by University of Cambridge on 15/09/2017 15:34:56.

expected to be on the order of 1 cm/s for $\eta_w \approx 1$ Pa.s, in fair agreement with values in figure 1d. Hence eq. (2) captures the simple regime where dissipation mainly occurs in the drop. It could have been more complicated. As drops spread or move, dissipation often concentrates close to the contact line, which we did not consider: the apparent contact angle here is large and the real contact angle (hidden by the oil meniscus) even larger [25, 27], which minimizes dissipation in the water wedge. Moreover, even for modest slip at the drop scale, the local slip number $\sigma_w = \eta_w h/\eta_o H$ (where we introduce a typical local thickness H), can become arbitrarily large close to the wedge ($H \to 0$), which minimizes even more wedge friction.

In the opposite limit where oil is more viscous than water ($\eta_o > \eta_w$, figure 1e), the drop velocity is not anymore linear in driving force. Dissipation is expected to take place in oil, that is, in the underlying film and in the surrounding meniscus. Let us discuss the corresponding frictions. (i) The typical velocity gradient in the film scales as V_i/h (figure 2b), which yields a friction $F_o \sim \eta_o V_i R^2/h$. For $\eta_w < \eta_o$, the slip number $\sigma = \eta_w h/\eta_o R$ is small compared to unity and the interface velocity V_i in eq. (1) reduces to σV. After injecting this value in the expression of F_o, we get a force scaling as $\eta_w VR$, of the same form, surprisingly, as in the limit $\eta_w > \eta_o$. Viscous oils are hardly displaced by water, and the corresponding friction is that in the drop, independent of the oil viscosity η_o, in contradiction with the two plateaus in figure 2a. (ii) As emphasized above, liquids on lubricant-infused materials are surrounded by a "foot" sketched and observed in figures 1a, 1b and 1c. If we designate its typical size by ℓ, we can first consider that the motion generates a stress $\eta_o V/\ell$ in the meniscus. Once integrated over the its surface area $R\ell$, we find the Stokes force $F_o \sim \eta_o VR$ first proposed by Smith *et al*. [21]. This formula provides a speed linear in driving force, in contradiction with the data in Figure 1e. We correct this approach by considering the dynamic nature of this meniscus, which is constantly pushed by the moving drop (figures 1c and 2c). A wedge of oil completely wets a substrate made of the same liquid. Hence its dynamic contact angle θ is given by Tanner's law [2-3, 28], $\theta \approx (\beta \eta_o V/\gamma_o)^{1/3}$, where β is a numerical factor that reflects the singular dissipation at the wedge tip. Integrating the viscous stress in this region provides $\beta \approx \ln(\ell/\varepsilon)$ where ε is the typical thickness of the layer of wetting oil on which the wedge glides. It is here given by the size of the Glaco beads (about 30 nm) so that we expect β to be of order 10. As shown by Huh and Scriven [2], the wedge friction (per unit length) scales as $\beta \eta_o V/\theta$, which yields a force $F_o \sim \beta(\eta_o V/\theta)R$ once it is integrated over the drop perimeter.

Soft Matter Accepted Manuscript

View Article Online
DOI: 10.1039/C7SM01226H

Plugging Tanner's law in the latter formula gives: $F_o \sim \gamma_o R(\beta\eta_o V/\gamma_o)^{2/3}$, which is non-linear in velocity. Its balance with gravity provides a speed of descent varying as $\sin^{3/2}\alpha$, in agreement with figure 1e (coloured, dashed lines). Our data also show that the speed in this regime is sensitive to the texture density ϕ. This is compatible with our interpretation: the wedge friction mainly takes place over the pillar tops, since oil glides on itself between the pillars. The distance to be considered for integrating the local stress $\beta\eta_o V/\theta$ becomes $2\pi\phi R$ instead of $2\pi R$, which eventually leads to $F_o \sim \gamma_o \phi R\,(\beta\eta_o V/\gamma_o)^{2/3}$. Hence we get:

$$(3) \qquad V \sim \frac{(\rho g)^{3/2} R^3}{\gamma_o^{1/2}\phi^{3/2}\beta\eta_o} \sin^{3/2}\alpha$$

We did not consider up to now the friction in the trailing side of the oil meniscus sketched in figure 2c, at the oil/water interface. This friction scales as $(\eta_o V/\varepsilon)\,\lambda R$, denoting ε and λ the thickness and length scale of the meniscus tail. Assuming a Laudau-Levich scaling, $\varepsilon \sim R(\eta_o V/\gamma_{ow})^{2/3}$ and $\lambda \sim R(\eta_o V/\gamma_{ow})^{2/3}$, the friction force F_o keeps the same scaling as previously ($F_o \sim \sin^{2/3}\alpha$), which does not modify our conclusions [29-31]. More quantitatively, the absence of singularity (thus of factor β) should make this additional friction smaller than the wedge one.

Eq. (3) nicely captures the experimental observations. (i) A meniscus friction provides a power law with exponent 3/2 between velocity and driving force, in accord with figure 1e. (ii) As also observed, the denser the texture, the smaller the speed: the positions of the lines in figure 1e were chosen as to obey the $\phi^{3/2}$-dependency predicted by eq. (3). The fit is found to be convincing even if the model at the highest density slightly underestimates observed speeds. (iii) We understand why V is inversely proportional to the oil viscosity η_o (the more viscous the wedge of oil, the slower the drop), as reported in figure 2a. (iv) We can finally check the unusual dependency of the speed with drop size, in R^3 instead of R^2 for Stokes' law. In figure 2d, the speed in this regime is plotted as a function of $\sin\alpha$ for drop volumes $\Omega \sim R^3$ varying between 1 μL and 40 μL. As expected from eq. (3), the larger the drop, the quicker it is. The agreement is quantitative: fits in the figure (dotted lines) are calculated by taking coefficients proportional to the drop volume (eq. 3), which leads to a very satisfactory agreement with all the data.

Published on 08 September 2017. Downloaded by University of Cambridge on 15/09/2017 15:34:56.

Soft Matter Accepted Manuscript

View Article Online
DOI: 10.1039/C7SM01226H

Published on 08 September 2017. Downloaded by University of Cambridge on 15/09/2017 15:34:56.

Depending on the contrast in viscosity between oil and water, we discussed two mechanisms of dissipation, and our curves in figures 1d and 1e suggest that drops on infused materials follow either of these laws. This is a consequence of the high viscosity contrasts in figure 1, where the ratio η_o/η_w is either 1/50 or 50. Conversely, figure 2a shows that the transition between both frictions can be directly evidenced by varying the water viscosity at fixed η_o. The transition takes place at a critical water viscosity $\eta*$, found in figure 2a to increase with η_o. By matching eqs. (2) and (3), we obtain $\eta* \sim a\eta_o$, where the number $a = \gamma_o^{1/2}\phi^{3/2}/(\rho g)^{3/2}R \sin^{1/2}\alpha$, is expected in our systems to be of order unity. $\eta*$ scales as the oil viscosity η_o, as observed in figure 2a.

Another way to discuss the transition between the two regimes of dissipation consists of performing experiments with liquids having similar viscosities. In figure 2e, we plot the descent velocity V as a function of the tilt angle α for $\eta_o = 100$ mPa.s and $\eta_w = 500$ mPa.s. Contrasting with the plots in figure 1, V now successively follows dependencies in $\sin^{3/2}\alpha$ and in $\sin\alpha$, in agreement with our discussion: the two frictions coexist, but oil friction should dominate water friction at low speed. Matching eqs. (2) and (3) now provides a transition speed $V* \sim \phi\gamma_o\eta_o^2/\eta_w^3$, on the order of a few millimetres per second for the parameters of this experiment – in excellent agreement with the data, and increasing with ϕ, as observed in figure 2d. Conversely, in the limits $\eta_o << \eta_w$ (or $\eta_o >> \eta_w$), $V*$ rapidly tends to zero (or infinity), so that the whole set of data corresponds to the water-dominated (or oil-dominated) regime, as in figure 1.

When oil imposes the friction law, we also observe in figure 1e a critical descent velocity above which V is larger than predicted by eq. (3) – a regime illustrated by the supplementary movie 4. Friction in this fast regime is different, and smaller. The transition speed in figure 1e is around 2 cm/s, which results in a capillary number (in oil) $\eta_o V/\gamma_o$ of order 0.1. At such a capillary number, Tanner's law predicts that the advancing dynamic angle is around 90° [32], which implies that the Huh-Scriven assumption of an acute wedge is not valid anymore, and explains why wedge dissipation can be minimized. As a tentative model for this quick regime, we assume that the oil meniscus becomes fully dynamical: it is constantly extracted from the texture by water surface tension γ_w before being reinjected at a velocity of order V below the drop. This interpretation explains how the velocity can become independent of the texture

Soft Matter Accepted Manuscript

View Article Online
DOI: 10.1039/C7SM01226H

density ϕ: water being lubricated by a thick dynamic film of oil, the texture gets erased. Oil is drawn at a velocity scaling as γ_w/η_o that must exceed the drop velocity, that is, $\eta_o V/\gamma_w < 1$. This condition is satisfied at capillary numbers $\eta_o V/\gamma_o < 0.1$. The dynamic meniscus, of unknown size r, deposits a film with thickness ε, for which we assume a Landau-Levich scaling, $\varepsilon \sim r\,(\eta_o V/\gamma_{ow})^{2/3}$. While the front edge of the meniscus is sharp and minimizes dissipation, the viscous force present in the deposition region scales as $(\eta_o V/\varepsilon)rR \sim \gamma_{ow} R(\eta_o V/\gamma_{ow})^{1/3}$, which indeed yields a descent velocity varying as $\sin^3\alpha$ (figure 1e). This regime intersects the previous one when frictions are comparable, that is, at a velocity scaling as $\gamma_{ow}^2/\phi\gamma_o\eta_o$ that depends on ϕ, as observed in figure 1e.

We finally test the robustness and generality of our findings by considering similar experiments on samples with smooth pillars instead of rough pillars. This induces a significant adhesion and the tilt angle $\alpha^*(\phi)$ for drop departure becomes for instance 15° for $\phi = 23\%$ (and $\Omega = 20$ µL). This angle expresses the balance of gravity with pinning, so that our equations must be corrected by considering an effective slope ($\sin\alpha - \sin\alpha^*$) instead of $\sin\alpha$. This simple fact limits the range of explored driving forces, and makes it more difficult to establish firm scaling laws. Yet, as seen in figure 3, our main conclusions remain valid. For viscous water ($\eta_w > \eta_o$), the speed is linear with the driving force (figure 3a), as expected in a regime where dissipation occurs in the drop. In the opposite case ($\eta_o > \eta_w$), dissipation mainly occurs in oil, and we recover the power law in 3/2 (with scattered data, due to adhesion), the dependency in texture density ϕ, and the quick regime at large α (figure 3b). As highlighted in figure 3c, it is worth noticing that the friction in the latter regime becomes independent of the surface adhesion expressed by α^*: data for $\alpha^* = 0$ and for $\alpha^* = 15°$ superimpose at large tilt in this self-lubricating regime, which confirms that surface topology has no more any impact on the dissipation at large α. The figure finally allows us to directly compare the speed of the drops in the main regime of oil dissipation ($\sin\alpha < 0.7$): water moves much slower (by a factor that can be typically 10) when adhesion is present, a consequence of the reduction of driving force in this case. This shows that textured, infused materials are not always ultra-slippery *per se*, but need to be designed so that the water/solid interface is minimized, as done here with the sub-nanotexture.

Published on 08 September 2017. Downloaded by University of Cambridge on 15/09/2017 15:34:56.

Soft Matter Accepted Manuscript

View Article Online
DOI: 10.1039/C7SM01226H

Beyond the asymptotic scalings described so far, we can finally try to capture all our results by simply adding the two independent sources of friction at intermediate tilt angles ($\sin\alpha < 0.7$). Drop velocity is deduced from the balance of the driving force with the total friction force written as $bF_o + cF_w$, where b and c are two numbers. This calculated velocity is plotted in figure 3d for the data obtained with nude pillars, and found to be nicely described by our equations provided we choose $b = 13 \pm 1$ and $c = 11 \pm 1$. Even if these numbers remain to be explicitly calculated, we can emphasize here that the model quantitatively succeeds at describing all the experiments with a unique set of numerical parameters b and c.

Published on 08 September 2017. Downloaded by University of Cambridge on 15/09/2017 15:34:56.

Soft Matter Accepted Manuscript

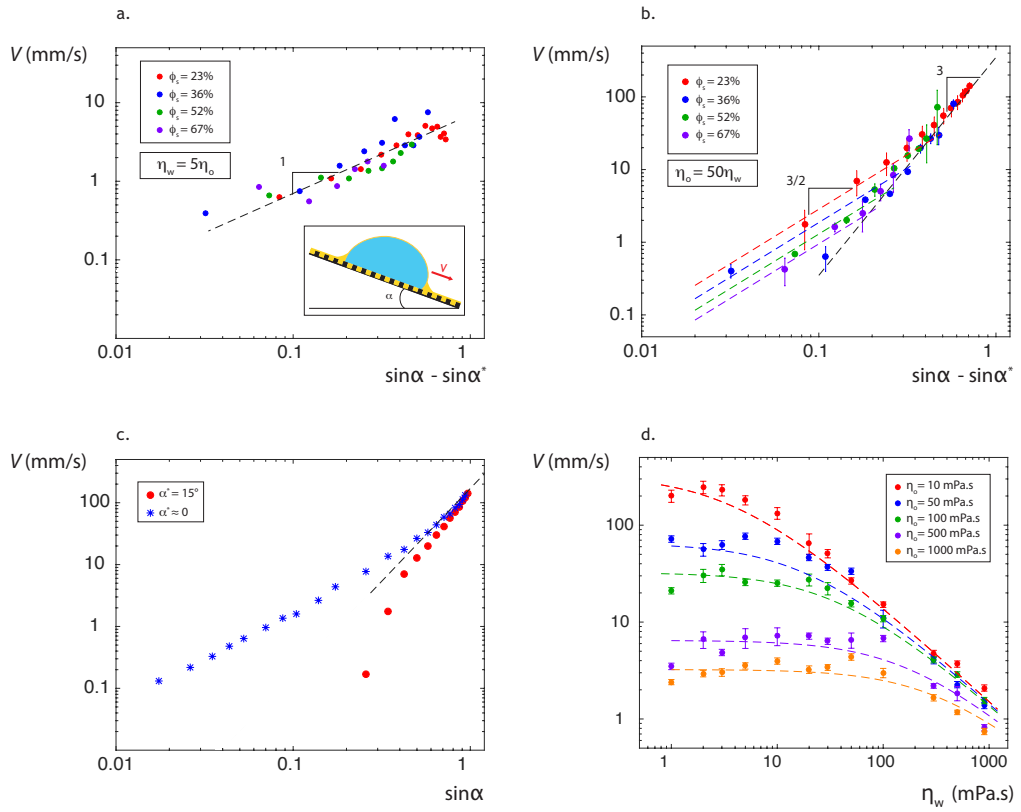

Figure 3. **(a)** Drop speed V as a function of the driving parameter $\sin\alpha - \sin\alpha^*$, for $\eta_o = 100$ mPa.s and $\eta_w = 500$ mPa.s ($\eta_w > \eta_o$). The volume of the drop is $\Omega = 20\ \mu$L. The sketch in the inset highlights the existence of a direct contact between water and textures in these experiments. Pillar densities are $\phi = 23\%$ (red), $\phi = 36\%$ (blue), $\phi = 52\%$ (green) and $\phi = 67\%$ (purple). Even if α^* depends on ϕ, all data collapse on a single curve with slope 1 (dashed line). **(b)** In the opposite limit $\eta_o > \eta_w$ (here $\eta_w = 2$ mPa.s and $\eta_o = 100$ mPa.s; $\Omega = 20\ \mu$L), the drop mobility is not anymore linear in driving force. Dashed lines successively show the slopes 3/2 and 3, and colours correspond to $\phi = 23\%$ (red data), $\phi = 36\%$ (blue data), $\phi = 52\%$ (green data) and $\phi = 67\%$ (purple data). **(c)** Speed V as a function of $\sin\alpha$ for substrates with (blue) and without (red) sub-structures. Data collapse at high tilting angles, showing that pillars no longer play a role in this regime. **(d)** Speed V as a function of the drop viscosity η_w for various lubricant viscosities η_o, $\phi = 23\%$, $\alpha = 40°$ and $\Omega = 20\ \mu$L. Dashed lines show the speed expected when assuming a total friction $F = 13F_o + 11F_w$, where F_w and F_o are given by eqs (2) and (3).

View Article Online
DOI: 10.1039/C7SM01226H

Textured-infused materials are often qualified as "slippery", a term that both refers to the low adhesion of drops on such surfaces, and to the potential slip generated during the motion. Yet, we showed that dissipation for a millimetre-size drop remains classical (Stokes-like) in the limit where slip might import ($\eta_o < \eta_w$). The characteristic size of the drop is typically one hundred times larger than the lubricant thickness, which limits the influence of slip. In a Hele-Shaw cell, for instance, the size of the drop can be reduced to that of the texture, which should magnify slip and trigger new friction laws. In the opposite limit ($\eta_o > \eta_w$), dissipation mainly occurs in oil, yet not in the subjacent film (as we could think *a priori*), and we interpreted the observed non-linear friction by viscous effects in the front edge of the meniscus surrounding the drop. As the driving force is increased, the wedge dissipation is suddenly suppressed, which leads to a third dynamical regime that seems to arise from the self-lubrication of the drop. In all these regimes, the lubricant was found to induce specific friction laws, mostly related to the existence of a circular meniscus around the drop. This should be general, in particular at high speeds, and our study might help to understand the behaviour of drops at impact [33] or the way a liquid film dewets on lubricant-infused materials. We would finally be happy to extend these findings to the dynamics of solid objects when they meet such surfaces, a situation for which slip was observed to be spectacular as seen when ants get trapped by infused plant surfaces [17-18].

Published on 08 September 2017. Downloaded by University of Cambridge on 15/09/2017 15:34:56.

Soft Matter Accepted Manuscript

Acknowledgements

This work has received the support of Institut Pierre-Gilles de Gennes (équipement d'excellence, "Investissements d'avenir", programme ANR-10-EQPX-34).

References

1. Joanny J.F. and de Gennes, P.G. A model for contact angle hysteresis, *J. Chem Phys.* **81,** 552– 562 (1984).
2. Huh C. and Scriven L.E. Hydrodynamic model of steady movement of a solid/liquid/fluid contact line, *J. Colloid Interface Sci.*, **35,** 85–101 (1971).
3. Snoeijer J.H. and Andreotti B. Moving contact lines: scales, regimes, and dynamical transitions*, Annu. Rev. Fluid Mech*. **45,** 269–292 (2013).
4. Leidenfrost J.G. De Aqua Communis Nonnullis Qualitatibus Tractatus. Impensis Hermanni Ovenni, Univers. Bibliopolae, Duisbourg (1756).
5. Ybert C., Barentin C., Cottin-Bizonne C., Joseph P., and Bocquet L. Achieving large slip with superhydrophobic surfaces: Scaling laws for generic geometries, *Phys. Fluids*, **19,** 123601 (2007).
6. Rothstein J.P. Slip on superhydrophobic surfaces, *Annu. Rev. Fluid Mech*. **42,** 89–109 (2010).
7. Quéré D. Non-sticking drops. *Rep. Prog. Phys.* **68,** 2495–2533 (2005).
8. Irajizad P., Hasnain M., Farokhnia N., Sajadi S.M. and Ghasemi H. Magnetic slippery extrême icephobic surfaces, *Nat. Comm.* **7,** 13395 (2016).

View Article Online
DOI: 10.1039/C7SM01226H

9. Epstein A.K., Wong T.S., Belisle R.A., Boggs E.M. and Aizenberg J. Liquid-infused structured surfaces with exceptional anti-biofouling performance. *Proc. Natl Acad. Sci. USA* **109,** 13182–13187 (2012).
10. Anand S., Paxson A.T., Dhiman R., Smith J.D. and Varanasi K.K. Enhanced condensation on lubricant-impregnated nanotextured surfaces. *ACS Nano* **6,** 10122–10129 (2012).
11. Anand S., Rykaczewski K., Subramanyam S.B., Beysens D. and Varanasi K.K. How droplets nucleate and grow on liquids and liquid-impregnated surfaces. *Soft Matter* **11,** 69–80 (2015).
12. Kim P., Wong T.S., Alvarenga J., Kreder M.J., Adorno-Martinez W.E. and Aizenberg J. Liquid-infused nanostructured surfaces with extreme anti-ice and anti-frost performance. *ACS Nano* **6,** 6569–6577 (2012).
13. Stone H.A. Ice-Phobic Surfaces That Are Wet. *ACS Nano* **6,** 6536–6540 (2012).
14. Subramanyam S.B., Rykaczewski K. and Varanasi K.K. Ice adhesion on lubricant-impregnated textured surfaces. *Langmuir* **29,** 13414–13418 (2013).
15. Barthlott W., Neinhuis C., Cutler D., Ditsch F., Meusel I., Theisen I. and Wilhelmi H. Classification and terminology of plant epicuticular waxes, *Bot. J. Linnean* **126,** 237–260 (1998).
16. Koch K. and Barthlott W., Superhydrophobic and superhydrophilic plant surfaces: an inspiration for biomimetic materials, *Phil. Trans. R. Soc.* **367,** 1487–1509 (2009).
17. Bohn H.F. and Federle W. Insect aquaplaning: Nepenthes pitcher plants capture prey with the peristome, a fully wettable water-lubricated anisotropic surface, *Proc. Natl Acad. Sci. USA,* **101,** 14138–14143 (2004).
18. Bauer U., Bohn H.F. and Federle W., Harmless nectar source or deadly trap: Nepenthes pitchers are activated by rain, condensation and nectar, *Proc. R. Soc.* **275,** 259–265 (2008).
19. Wong T.S., Kang S.H., Tang S.K., Smythe E.J., Hatton B.D., Grinthal A. and Aizenberg J. Bioinspired self-repairing slippery surfaces with pressure-stable omniphobicity. *Nature* **477,** 443–447 (2011).
20. Lafuma A. and Quéré D. Slippery pre-suffused surfaces. *EPL* **96,** 56001 (2011).
21. Smith J.D., Dhiman R., Anand S., Reza-Garduno E., Cohen R.E., McKinley G.H. and Varanasi K.K. Droplet Mobility on Lubricant-Impregnated Surfaces, *Soft Matter*, **9,** 1772–1780 (2013).
22. Courbin L., Bird J.C., Reyssat M. and Stone H.A. Dynamics of wetting: from inertial spreading to viscous imbibition *J. Phys. Condens. Matter* **21,** 464127 (2009).
23. Seiwert J., Clanet C. and Quéré D. Coating of a textured solid. *J. Fluid Mech.* **669,** 55–63 (2011).
24. Liu Y., Wexler J.S., Schönecker C. and Stone H.A. Effect of viscosity ratio on the shear-driven failure of liquid-infused surfaces *Phys. Rev. Fluids* **1,** 074003 (2016).
25. Semprebon C., McHale G. and Kusumaatmaja H. Apparent contact angle and contact angle hysteresis on liquid infused surfaces, *Soft Matter*, **13,** 101–110 (2017).
26. Guan J.H., Gutierrez E.R., Xu B., Wood D., McHale G., Aguilar R.A.L. and Wells G.G. Drop transport and positioning on lubricant impregnated surfaces *Soft Matter* **13**, 3404–3410 (2017).
27. Schellenberger F., Xie J., Encinas N., Hardy A., Klapper M., Papadopoulos P., Butt H.J. and Vollmer D. Direct observation of drops on slippery lubricant-infused surfaces. *Soft Matter* **11,** 7617–7626 (2015).
28. Tanner L. The spreading of silicone oil drops on horizontal surface *J. Phys. D* **12,** 1473–1484 (1979).
29. Bico J. and Quéré D. Falling slugs, *J. Colloid Interface Sci.* **243,** 262–264 (2001).
30. Reyssat E. Drops and bubbles in wedges, *J. Fluid Mech.,* **748,** 641–662 (2014).
31. Cantat I. Liquid meniscus friction on a wet plate: bubbles, lamellae and foams, *Phys. Fluids* **25,** 031303 (2013).
32. Hoffman R.L. A study of the advancing interface. I. Interface shape in liquid-gas systems. *J. Colloid Interface Sci.*, **50,** 228–241 (1975).
33. Kim J.H. and Rothstein J.P. Droplet impact dynamics on lubricant-infused superhydrophobic surfaces: The role of viscosity ratio. *Langmuir* **32,** 10166–10176 (2016).

Published on 08 September 2017. Downloaded by University of Cambridge on 15/09/2017 15:34:56.

Soft Matter Accepted Manuscript

View Article Online
DOI: 10.1039/C7SM01226H

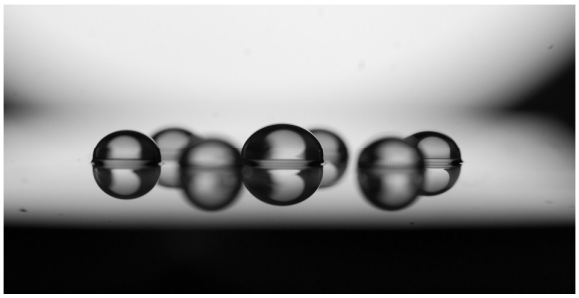

We discuss the special laws of friction observed as a drop glides on a liquid-infused material.

Published on 08 September 2017. Downloaded by University of Cambridge on 15/09/2017 15:34:56.

Soft Matter Accepted Manuscript